Linear analysis of a multibeam cyclotron-resonance maser array

M. Korol and E. Jerby
Faculty of Engineering, Tel Aviv University, Ramat Aviv, 69978, Israel
(Received 30 October 1996)

The multibeam cyclotron-resonance maser (CRM) array is a new concept for compact, high-power CRM devices operating at low voltages. The CRM array studied in this paper employs low-energy electron beams, which are propagating in coupled channels in a two-dimensional periodic waveguide. A static magnetic field spirals the electrons in synchronism with a spatial harmonic of the electromagnetic wave. A matrix gain-dispersion equation of the CRM-array interaction is derived in the paper. Numerical examples are presented for a comparison between CRM interactions of one, two, and three electron beams with various waveguide modes. The analysis shows that the multibeam cyclotron interaction yields a considerable gain of microwaves in selective modes. [S1063-651X(97)09204-0]

PACS number(s): 41.60.−m, 84.40.Ik, 52.35.Qz, 52.35.Hr

I. INTRODUCTION

Advanced sources of high-power microwaves (HPM) are needed for scientific and technological purposes. HPM devices are key elements in the development of novel particle accelerators, fusion reactors, radars, communication systems, and various industrial and medical processes. Cyclotron-resonance masers (CRMs) and free-electron masers (FEMs) have been studied intensively as HPM amplifiers and oscillators [1,2]. Both CRM and FEM mechanisms are based on resonant interactions between the amplified electromagnetic (em) wave and an electron beam.

The CRM resonance condition between an em wave and a copropagating electron beam is given by

$$\omega \sim \omega_c + k_z V_z , \tag{1}$$

where ω and k_z are the em-wave frequency and axial wave number, respectively, and V_z is the axial electron velocity. The relativistic angular cyclotron frequency is $\omega_c = eB_0/\gamma m_0$, where e, m_0, and γ are the electron charge, rest mass, and relativistic factor, respectively, and B_0 is the axial static magnetic field [3,4]. The CRM interaction with a fast em wave ($k_z \leqslant \omega/c$) requires a nonzero initial transverse velocity in order to amplify the em wave. The fast-wave CRM interaction stems from the azimuthal electron bunching in the spiral electron trajectories caused by the transverse electric field component of the em wave [5].

Recent CRM studies are devoted to nonlinear analysis [6,7], multimode analysis [8], high cyclotron-harmonic operation [7,9–11], short-pulse generation [12], and to the development of high-power generators [10,13–15]. Various prebunching mechanisms and gyroklystrons [8–10,15] have been investigated in order to increase efficiency.

Dielectric-loaded cyclotron masers [16–18] are developed in order to extend the slow-wave ($k_z > \omega/c$) tunability and to reduce the required electron energy. The slow-wave CRM interaction is characterized by an axial electron bunching effect, known as the Weibel mechanism [5,17,19]. The anomalous Doppler effect [20–22] can be realized in a slow-wave cyclotron with a zero initial transverse electron velocity.

The periodic-waveguide cyclotron (PWC) maser is a device in which the interaction occurs in a periodically loaded waveguide [23,24]. It combines the properties of fast- and slow-wave CRM interactions. The artificial dielectric properties of the periodic waveguide allow operation of the PWC device in new parametric regimes. In particular, a quasi-anomalous Doppler effect is feasible in periodic waveguides with low harmonic impedance [25]. Experimental and theoretical studies [23–29] show that the PWC has the potential to become a compact low-voltage source of microwaves. For instance, the PWC-oscillator experiment conducted by Jerby *et al.* [27] employs an 8 keV, 200 mA electron beam, and its output power is >0.4 kW, which corresponds to a $>25\%$ efficiency.

Most of the HPM generators employ a single high-energy electron beam. For instance, a gyrotron producing 3 MW power at 140 GHz frequency with a 45% efficiency [30] employs an electron beam of 95 keV and 84 A. A cyclotron autoresonance maser (CARM) oscillator experiment reported in Ref. [31] generates 13 MW output power at 38 GHz with an $\sim 25\%$ efficiency employing a 500 keV, 100 A electron beam. Using a single high-current electron beam limits the output radiation power by the beam energy and current. The interaction is impeded by space-charge effects, and, in addition, the device overhead required for a single high-power electron beam is fairly large (high-voltage power supplies, huge electron gun and collector, shielding system, etc.). The use of an array of low-current (high-perveance) electron beams may alleviate some of these difficulties.

A two-beam cyclotron maser was proposed and studied in Ref. [32]. The beams propagate with different stream velocities in the cylindrical waveguide. The interaction between the fast transverse plasma wave of one beam and the slow transverse plasma wave of the other beam results in rf power gain. The radiation frequency is inversely proportional to the energy difference between the beams. Consequently, the high-frequency radiation can be achieved for low electron energies and axial magnetic fields. Numerical simulations predict an 80 dB/m gain at 50 GHz for two nonrelativistic beams with a 23 A/cm^2 current of each one, an 87.5 keV mean electron energy, and a 25 keV difference between the beams.

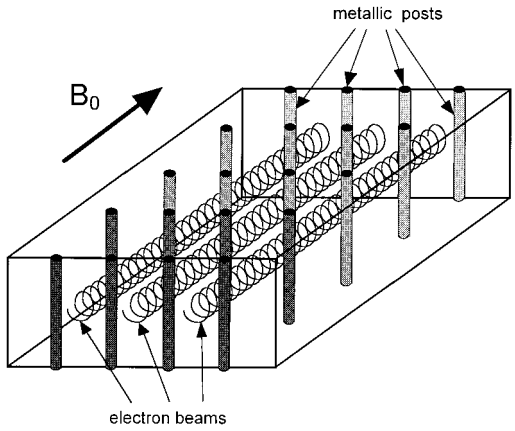

FIG. 1. Schematic of the multibeam CRM array in a 2D periodic waveguide.

The cluster klystron [33] is proposed for linear colliders. The experimental model consists of three parallel electron beams with equal 33 A current and 370 keV energy. The device produces 78 MW output power with a 70% efficiency. The efficiency is larger by a factor of 2 comparing with a conventional klystron employing one 100 A electron beam.

The concept of the CRM array was proposed [28] as a multibeam extension of the PWC scheme in order to produce high-power microwaves by many low-energy electron beams propagating in parallel directions. The device consists of a multichannel lattice waveguide as shown in Fig. 1. The electron beams pass through the different channels and interact with the spatial em-wave harmonics, due to the axial magnetic field. The various channels of the CRM array are coupled to each other. Synergistic effects are expected in this device. The two-dimensional (2D) CRM array shown in Fig. 1 is being studied experimentally by Lei and Jerby [29]. It employs a rectangular waveguide with a matrix of inductive metal posts inside. The parameters of this waveguide are studied in Ref. [34]. Electron beams with various axial velocities are injected simultaneously into the waveguide. Each electron beam flows between two adjacent rows of metal posts. Its current is relatively small and therefore the space-charge effects are negligible.

The practical advantages of the proposed scheme are (a) the low-voltage, low-current operation of the separated electron beams, and consequently (b) the alleviation of space-charge effects, and (c) the feasibility of high-power microwave generation by a compact device.

The concept of the CRM array can be extended to three-dimensional arrays. It can be developed even further to new concepts of a multibeam CRM interaction in a *photonic-band-gap* structure [35], and of a phased-array radiator [36,37].

This paper presents theoretical analysis and numerical calculations of the 2D PWC array. This analysis is a multimode extension of a CRM model in periodic waveguides [24]. The 2D periodic-waveguide analysis is based here on the microwave theory approach [38,39]. The gain-dispersion equation of the convective PWC interaction is derived in the next section. This equation relates the output and input amplitudes of the amplified em-wave signal as a function of the interaction parameters. A multimode analysis of the periodic waveguide is presented in Sec. III. A numerical analysis of the PWC-array amplification with different number of electron beams and in different em modes is presented in Sec. IV.

II. DERIVATION OF THE CRM-ARRAY GAIN-DISPERSION RELATION

The em wave in the 2D periodic waveguide shown in Fig. 1 is described as a superposition of linearly independent TE_{n0} modes [38] (in this analysis, we assume that the wave profile is uniform in the x dimension). Each mode is expanded to an infinite set of spatial harmonics, and is characterized by its repetitive transverse profile and axial wave number in each unit cell of the periodic waveguide. The harmonic profiles and axial wave numbers are determined by a dispersion equation for each transverse mode [38]. Hence the em wave in the periodic waveguide is expressed in the form

$$H_y(\omega,y,z)=\sum_{n=1}^{\infty} A_n(z)\sum_{k=-\infty}^{\infty} h_{nk}\psi_{nk}(y)e^{-j\beta_{nk}z}, \quad (2a)$$

$$E_x(\omega,y,z)=\sum_{n=1}^{\infty} A_n(z)\sum_{k=-\infty}^{\infty} e_{nk}\psi_{nk}(y)e^{-j\beta_{nk}z}, \quad (2b)$$

where $A_n(z)$ is the slowly varying amplitude of the nth periodic-waveguide mode, the subscripts n and k denote mode and harmonic orders, respectively, e_{nk} and h_{nk} are electric and magnetic harmonic coefficients, respectively, and $\psi_{nk}(y)$ and β_{nk} are their transverse profile and axial wave number, respectively. The normalized harmonic impedance is defined as

$$\hat{Z}_{nk}=\frac{e_{nk}}{h_{nk}}Z_0^{-1}, \quad (3)$$

where $Z_0=\sqrt{\mu_0/\epsilon_0}$ is the free-space wave impedance. Expressions for the mode coupling and amplitude variation due to the cyclotron interaction are derived in this section.

Following Ref. [24], the wave equation for the transverse magnetic component of the nth mode is given in the complex Laplace space by

$$\left(\frac{\partial^2}{\partial y^2}+k_0^2+s^2\right)\tilde{H}_{yn}(\omega,s)-\left(s+\frac{\partial}{\partial z}\right)H_{yn}(\omega,z=0) = -s\sum_{n'=1}^{\infty}\tilde{J}_{xn'}(\omega,s), \quad (4)$$

where $k_0=\omega/c$ is the free-space wave number and s is a complex Laplace variable. Using the method of characteristic lines, the electron current $\tilde{J}_{xn'}$ induced by the n'th waveguide mode is given [24] by

$$\widetilde{J}_{xn'}(\omega,s)=\frac{\pi e^2}{m_0}\int_{P_{0\perp}}\int_{P_{0z}}\frac{P_{0\perp}}{\gamma}\left\{\frac{\widetilde{E}_{xn'}(\omega,s)-(P_{0z}/\gamma m_0)\mu_0\widetilde{H}_{yn'}(\omega,s)}{j\omega-j\omega_c+(P_{0z}/\gamma m_0)s}\right.$$
$$\left.-\frac{P_{0\perp}^2}{2\gamma^2 m_0^2}\frac{(j\omega/c^2)\widetilde{E}_{xn'}(\omega,s)+s\mu_0\widetilde{H}_{yn'}(\omega,s)}{[j\omega-j\omega_c+(P_{0z}/\gamma m_0)s]^2}\right\}f_0(P_{0z},P_{0\perp},x_0,y_0)dP_{0\perp}dP_{0z}. \quad (5)$$

The axial and azimuthal components of the initial electron momentum are P_{0z} and $P_{0\perp}$, respectively, x_0 and y_0 are the initial coordinates of electron, and f_0 is the zero-order electron distribution function.

The distribution function of an array of I electron beams, neglecting energy spread and emittance, is given by

$$f_0(P_{0z},P_{0\perp},x_0,y_0)=\frac{1}{2\pi\overline{P_{0\perp}}}\delta(P_{0\perp}-\overline{P_{0\perp}})\delta(P_{0z}-\overline{P_{0z}})\sum_{i=1}^{I}\overline{n_{0i}}g_{0i}(x_0,y_0), \quad (6)$$

where $\overline{n_{0i}}$ and $g_{0i}(x_0,y_0)$ are the ith electron-beam density and transverse profile, respectively, and the bars denote average initial values. Assuming electron beams with a circular and transversely uniform cross section, the profile function is given by

$$g_{0i}(x_0,y_0)=\begin{cases}1, & (x_0-x_{0i})^2+(y_0-y_{0i})^2<r_{0i}^2\\ 0, & \text{else,}\end{cases} \quad (7)$$

where r_{0i}, x_{0i}, and y_{0i} are the initial radius and the center coordinates, respectively, of the ith electron beam. Equations (2)–(6) result in a gain-dispersion equation of the nth-mode CRM-array interaction as follows:

$$\sum_{k=-\infty}^{\infty}[(\beta_{nk}^2+s^2)\widetilde{A}_n(s+j\beta_{nk})-(s-j\beta_{nk})A_{n0}]h_{nk}\psi_{nk}(y)=-\frac{s}{2c^2}\left(\sum_{i=1}^{I}\overline{\omega_{p0i}^2}g_{0i}(x_0,y_0)\right)\sum_{n'=1}^{\infty}\sum_{k'=-\infty}^{\infty}\left\{\frac{c\hat{Z}_{n'k'}-\overline{V_{0z}}}{j\omega-j\omega_c+\overline{V_{0z}}s}\right.$$
$$\left.-\frac{\overline{V_{0\perp}^2}}{2}\frac{jk_0\hat{Z}_{n'k'}+s}{(j\omega-j\omega_c+\overline{V_{0z}}s)^2}\right\}\widetilde{A}_{n'}(s+j\beta_{n'k'})h_{n'k'}\psi_{n'k'}(y), \quad (8)$$

where $\overline{V_{0z}}=\overline{P_{0z}}/\gamma m_0$ and $\overline{V_{0\perp}}=\overline{P_{0\perp}}/\gamma m_0$ are the axial and azimuthal electron velocities, respectively, and $\overline{\omega_{p0i}}=(e^2\overline{n_{0i}}/\gamma m_0\epsilon_0)^{1/2}$ is the relativistic plasma frequency associated with the ith electron beam. Using the orthogonality of modes and harmonics allows to reduce the transverse dependence of Eq. (8) by multiplying both sides by $\Sigma_n\Sigma_k e_{nk}^*\psi_{nk}\delta(s-j\beta_{nk})$ and integrating over the waveguide cross section. This results in

$$\sum_{k=-\infty}^{\infty}(s-2j\beta_{nk})p_{nk}[s\widetilde{A}_n(s)-A_{0n}]=-\frac{1}{2c^2}\sum_{n'=1}^{\infty}\sum_{k'=-\infty}^{\infty}(s-j\beta_{n'k'})\left(\sum_{i=1}^{I}\overline{\omega_{p0i}^2}F_{f_{n'k'i}}\right)\left\{\frac{c\hat{Z}_{n'k'}-\overline{V_{0z}}}{j(\omega-\omega_c-\beta_{n'k'}\overline{V_{0z}})+s\overline{V_{0z}}}\right.$$
$$\left.-\frac{1}{2}\overline{V_{0\perp}^2}\frac{jk_0\hat{Z}_{n'k'}+s-j\beta_{n'k'}}{[j(\omega-\omega_c-\beta_{n'k'}\overline{V_{0z}})+s\overline{V_{0z}}]^2}\right\}p_{n'k'}\widetilde{A}_{n'}. \quad (9)$$

The harmonic power flow p_{nk} and the filling factor of the ith electron beam, $F_{f_{nki}}$, are defined as

$$p_{nk}=h_{nk}e_{nk}^*\int_0^a\int_0^b\psi_{nk}^2(y)dxdy, \quad (10a)$$

$$F_{f_{nki}}=\frac{h_{nk}e_{nk}^*}{p_{nk}}\int_0^a\int_0^b g_{0i}(x,y)\psi_{nk}^2(y)dxdy, \quad (10b)$$

respectively, where a and b are the transverse dimensions of the rectangular waveguide. The products $p_{nk}F_{f_{nki}}$ are derived in Appendix A for electron beams with a circular and transversely uniform cross section.

We assume that the CRM resonance condition (1) is satisfied with the kth spatial harmonic of the nth waveguide mode. Consequently, the kth spatial harmonics of all the other modes are considered as close to the CRM resonance and are taken into account in the right side of Eq. (9). The other harmonics are assumed to be off-resonant and therefore neglected. Hence Eq. (9) is further reduced to

$$s\tilde{A}_n(s)-A_{0n}=-\frac{1}{2c^2}\left(\sum_{k'=-\infty}^{\infty}(s-2j\beta_{nk'})p_{nk'}\right)^{-1}\sum_{n'=1}^{\infty}\left(\sum_{i=1}^{I}\overline{\omega_{p0i}^2}F_{f_{n'ki}}\right)(s-j\beta_{n'k})p_{n'k}\left\{\frac{c\hat{Z}_{n'k}-\overline{V_{0z}}}{j(\omega-\omega_c-\beta_{n'k}\overline{V_{0z}})+s\overline{V_{0z}}}\right.$$
$$\left.-\frac{1}{2}\overline{V_{0\perp}^2}\frac{jk_0\hat{Z}_{n'k}+s-j\beta_{n'k}}{(j(\omega-\omega_c-\beta_{n'k}\overline{V_{0z}})+s\overline{V_{0z}})^2}\right\}\tilde{A}_{n'}(s). \tag{11}$$

Dimensionless operating parameters are introduced to simplify the equations. The CRM tuning parameter is given by

$$\hat{\theta}_{n'k}=(\omega-\omega_c-\beta_{n'k}\overline{V_{0z}})\frac{L}{\overline{V_{0z}}}, \tag{12}$$

and the space-charge parameter is defined as $\hat{\theta}_{pn'k}=[\Sigma_i\overline{\omega_{p0i}}\sqrt{F_{f_{n'ki}}}]L/\overline{V_{0z}}$ where L is the interaction length. The normalized wave number parameters are $\hat{k}_0=k_0L$ for free space, $\hat{\beta}_{nk}=\beta_{nkL}$ for the kth spatial harmonic, and $\hat{s}=jsL$ for the Laplace variable. Using these definitions, Eq. (11) is rewritten in the form

$$\hat{s}\tilde{A}_n(\hat{s})-A_{0n}=\frac{1}{2}\left(\sum_{k'=-\infty}^{\infty}(\hat{s}+2\hat{\beta}_{nk'})p_{nk'}\right)^{-1}\sum_{n'=1}^{\infty}\hat{\theta}_{pn'k}^2(\hat{s}+\hat{\beta}_{n'k})p_{n'k}\left\{\frac{\overline{\beta_{ez}}(\hat{Z}_{n'k}-\overline{\beta_{ez}})}{\hat{s}-\hat{\theta}_{n'k}}+\frac{\overline{\beta_{e\perp}^2}}{2}\frac{\hat{k}_0\hat{Z}_{n'k}-\hat{s}-\hat{\beta}_{n'k}}{(\hat{s}-\hat{\theta}_{n'k})^2}\right\}\tilde{A}_{n'}(\hat{s}), \tag{13}$$

where $\overline{\beta_{ez}}=\overline{V_{0z}}/c$ and $\overline{\beta_{e\perp}}=\overline{V_{0\perp}}/c$ are the normalized axial and azimuthal electron velocities, respectively.

Equation (13) holds for any waveguide-mode order n. Hence a matrix equation is derived for the relation between the column vectors $\underline{\tilde{A}}(\hat{s})=|\tilde{A}_n(\hat{s})|$ and $\underline{A_0}=|A_{n0}|$, as follows:

$$\left[\hat{s}[\hat{s}\underline{\underline{U}}-\underline{\underline{\hat{\Theta}}}_k]^2-\frac{1}{2}\underline{\underline{C}}_k(\hat{s})\underline{\underline{\hat{\Theta}}}_{pk}^2\left\{\overline{\beta_{ez}}[\hat{s}\underline{\underline{U}}-\underline{\underline{\hat{\Theta}}}_k][\underline{\underline{\hat{Z}}}_k-\overline{\beta_{ez}}\underline{\underline{U}}]+\frac{1}{2}\overline{\beta_{e\perp}^2}[\hat{k}_0\underline{\underline{\hat{Z}}}_k-\hat{s}\underline{\underline{U}}-\underline{\underline{\hat{\beta}}}_k]\right\}\right]\underline{\tilde{A}}=[\hat{s}\underline{\underline{U}}-\underline{\underline{\hat{\Theta}}}_k]^2\underline{A_0}. \tag{14}$$

The matrix parameters of Eq. (14) are defined as follows: U is a unit matrix, and $\underline{\underline{\hat{\beta}}}_k=|\hat{\beta}_{nk}|$ and $\underline{\underline{\hat{Z}}}_k=|\hat{Z}_{nk}|$ are diagonal matrices of harmonic wave numbers and impedances, respectively. The diagonal tuning and space-charge matrices are $\underline{\underline{\hat{\Theta}}}_k=|\hat{\theta}_{nk}|$ and $\underline{\underline{\hat{\Theta}}}_{pk}=|\hat{\theta}_{pnk}|$, respectively, and the nondiagonal power-flow matrix is

$$\underline{\underline{C}}_k(\hat{s})=|C_{n'n}^{(k)}(\hat{s})|=\left|\left(\sum_{k'=-\infty}^{\infty}(\hat{s}+2\hat{\beta}_{n'k'})p_{n'k'}\right)^{-1}\times(\hat{s}+\hat{\beta}_{nk})p_{nk}\right|. \tag{15}$$

Finally, the matrix gain-dispersion equation of the CRM-array interaction results in the Pierce-type fourth-order equation as follows:

$$\underline{\tilde{A}}(\hat{s})=\left[\hat{s}[\hat{s}\underline{\underline{U}}-\underline{\underline{\hat{\Theta}}}_k]^2-\frac{1}{2}\underline{\underline{C}}_k(\hat{s})\underline{\underline{\hat{\Theta}}}_{pk}^2\underline{\underline{Q}}_k(\hat{s})\right]^{-1}[\hat{s}\underline{\underline{U}}-\underline{\underline{\hat{\Theta}}}_k]^2\underline{A_0}, \tag{16}$$

where the diagonal coupling matrix $\underline{\underline{Q}}_k(\hat{s})$ is defined as

$$\underline{\underline{Q}}_k(\hat{s})=\overline{\beta_{ez}}[\hat{s}\underline{\underline{U}}-\underline{\underline{\hat{\Theta}}}_k][\underline{\underline{\hat{Z}}}_k-\overline{\beta_{ez}}\underline{\underline{U}}]+\frac{1}{2}\overline{\beta_{e\perp}^2}[\hat{k}_0\underline{\underline{\hat{Z}}}_k-\hat{s}\underline{\underline{U}}-\underline{\underline{\hat{\beta}}}_k]. \tag{17}$$

The resulting gain-dispersion equation (16) and the associated coupling matrix $\underline{\underline{Q}}_k(\hat{s})$, Eq. (17), are a multimode generalization of the single-mode analysis of the periodic-waveguide CRM interaction presented in Ref. [24]. Equations (16) and (17) describe the spatial evolution of the input em wave where its transverse modes are coupled by the cyclotron interaction. The poles $\hat{s}$ of Eq. (16) determine the shift of the kth harmonic wave numbers $\hat{\beta}_{nk}$ in the complex plane. The corresponding residues describe the variation of em-wave amplitudes $A_n(z=L)$ due to the CRM interaction. The different terms in Eq. (16) represent various effects. The coupling matrix $\underline{\underline{Q}}_k(\hat{s})$ describes the CRM interaction with the resonant harmonic. Its different terms (17) correspond to various operating regimes of the CRM interaction as reported in Ref. [24]. The space-charge matrix $\underline{\underline{\hat{\Theta}}}_{pk}$ represents the effect of electron current density on the CRM coupling (note that collective space-charge effects are not included in this model). The power-flow matrix $\underline{\underline{C}}_k(\hat{s})$ describes the distribution of the em-wave power among the different modes and their spatial harmonics.

In the single-mode limit, Eq. (16) is reduced to the scalar gain-dispersion equation [24] as follows:

$$\tilde{A}(\hat{s})=\frac{(\hat{s}-\hat{\theta}_k)^2}{\hat{s}(\hat{s}-\hat{\theta}_k)^2-\frac{1}{2}\hat{\theta}_{pk}^2C_k(\hat{s})\kappa_k(\hat{s})}A_0. \tag{18}$$

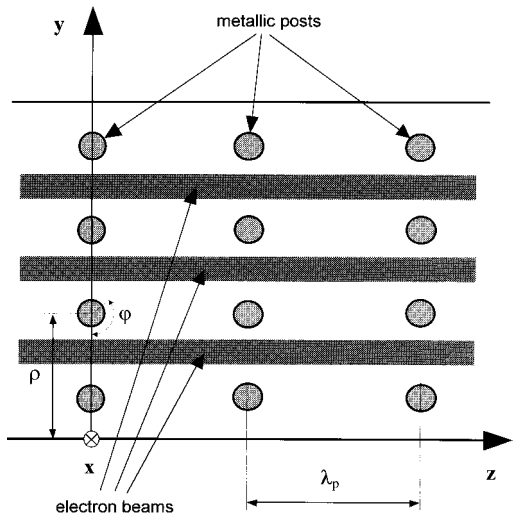

FIG. 2. The horizontal cross section of the 2D periodic waveguide.

The complex coupling coefficient, given by

$$\kappa_k(\hat{s}) = \overline{\beta_{ez}}(\hat{s}-\hat{\theta}_k)(\hat{Z}_k - \overline{\beta_{ez}}) + \frac{1}{2}\overline{\beta_{e\perp}^2}(\hat{k}_0\hat{Z}_k - \hat{s} - \hat{\beta}_k), \tag{19}$$

is a scalar analog of the coupling matrix $\underline{\underline{Q}}_k(\hat{s})$. The other parameters in Eqs. (18) and (19) are scalar analogs of the matrices in Eqs. (16) and (17), as well. The matrix gain-dispersion relation (16) and (17) derived in this section presents a general form of a CRM interaction in a multimode periodic waveguide.

III. DISPERSION ANALYSIS OF THE 2D PERIODIC WAVEGUIDE

The periodic waveguide shown in Fig. 1 is analyzed in this section in order to determine its modes and their spatial-harmonic characteristics (in the absence of the electron beams). Following Refs. [38,39], the analysis begins with a single unit cell, and then is generalized by the Floquet theorem to the entire periodic waveguide. The empty waveguide parameters (i.e., the spatial-harmonic wave number β_{nk}, power flow p_{nk}, and impedance $\hat{Z}_{nk}$) are required for the numerical solution of the matrix gain-dispersion equation (16) in the next section.

The horizontal cross section of the periodic waveguide is shown in Fig. 2. The unit cell of the periodic waveguide is determined by the axial period λ_p.

In this analysis, we assume that the radius of the metal posts, d, is small comparing to the waveguide width a. Consequently, the surface currents on the posts are directed nearly along their axis (i.e., the x axis in Fig. 2). Assuming that the incident waves are vertically polarized (as the TE_{m0} modes of the empty waveguide) the scattered waves from the vertical posts are composed of the same set of TE_{m0} modes. Other modes of the empty waveguide, including the $TE_{mm'}$ and $TM_{mm'}$ modes with $m' \neq 0$, are not supported then by the periodic waveguide, and therefore they

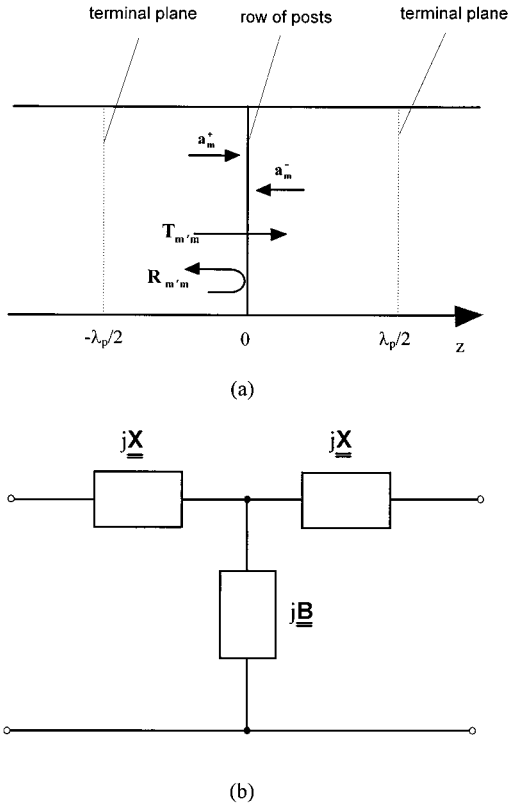

FIG. 3. A unit cell of the periodic waveguide: (a) Forward and backward em-wave components and the reflection and transmission coefficients. (b) An equivalent circuit of a unit cell.

are neglected in this analysis. This assumption is valid in the range $\pi md/2a \ll 1$. The resulting modes of the periodic waveguide are vertically polarized TE modes, as shown later in this section. In the other range, of higher modes or wide posts (i.e., where $md \sim 2a/\pi$), the analytical model should include the complete set of empty waveguide modes (i.e., all the $TE_{mm'}$ and $TM_{mm'}$ modes). In this case, which is not studied in this paper, the periodic-waveguide modes may not be purely TM or TE modes.

The transverse row of posts acts as a partial mirror on the incident em waves a_m^+ and a_m^-, as shown schematically in Fig. 3(a) (the superscripts $+$ and $-$ denote forward and backward waves, respectively). The total incident em wave is divided into even and odd components as follows:

$$E_x^{(i)}(y,z) = E_x^{(i,o)}(y,z) + E_x^{(i,e)}(y,z), \tag{20}$$

where the superscripts o and e denote the odd and even components of the incident electric field, respectively. These components are given by

$$E_x^{(i,o/e)}(y,z) = \sum_{m=1}^{\infty} a_m^{(o/e)} \sin\left(\frac{\pi m}{a} y\right)(e^{jk_m z} \mp e^{-jk_m z}), \tag{21}$$

where k_m is the axial wave number of the mth mode. The amplitudes $a_m^{(o/e)}$ of the odd and even mode are related to the amplitudes a_m^+ and a_m^- by

$$a_m^{\pm}=a_m^{(e)}\mp a_m^{(o)}. \tag{22}$$

In this analysis, the modes may be either propagating or evanescent.

The currents induced on the surface of posts generate the scattered em wave in order to satisfy the boundary conditions. This scattered wave is composed of various $\mathrm{TE}_{m'0}$ empty waveguide modes, which are identified by the integer m'. The multimode analysis of incident and scattered em waves is presented in Appendix B. It allows determination of the matrices of reflection and transmission coefficients for the odd and even modes. These matrices are shown in Fig. 3(a) as $R_{m'm}$ and $T_{m'm}$, respectively.

The equivalent transmission line circuit of a unit cell of the periodic waveguide is shown in Fig. 3(b). The matrices $j\mathrm{B}$ and $j\mathrm{X}$ are the equivalent reactive susceptances and reactances, respectively. They are related to the matrices of odd and even reflection coefficients as follows:

$$\underline{\underline{\mathrm{R}}}^{(o)}=(j\underline{\underline{\mathrm{X}}}+\underline{\underline{\mathrm{U}}})^{-1}(j\underline{\underline{\mathrm{X}}}-\underline{\underline{\mathrm{U}}}), \tag{23a}$$

$$\underline{\underline{\mathrm{R}}}^{(e)}=[j\underline{\underline{\mathrm{X}}}+2(j\underline{\underline{\mathrm{B}}})^{-1}+\underline{\underline{\mathrm{U}}}]^{-1}[j\underline{\underline{\mathrm{X}}}+2(j\underline{\underline{\mathrm{B}}})^{-1}-\underline{\underline{\mathrm{U}}}]. \tag{23b}$$

An analysis of the periodic loaded transmission line is presented in Ref. [38]. The column vectors of equivalent voltages and currents are defined there by

$$\underline{\mathrm{V}}=|V_m|=|a_m^{+}+a_m^{-}|, \tag{24a}$$

$$\underline{\mathrm{I}}=|I_m|=|a_m^{+}-a_m^{-}|, \tag{24b}$$

respectively. The transfer matrix through the obstacle is given by

$$\begin{bmatrix}\underline{\mathrm{V}}\\ \underline{\mathrm{I}}\end{bmatrix}_{z=0^-}=\begin{bmatrix}\underline{\underline{\mathrm{U}}}-\underline{\underline{\mathrm{X}}}\underline{\underline{\mathrm{B}}} & j\underline{\underline{\mathrm{X}}}(2\underline{\underline{\mathrm{U}}}-\underline{\underline{\mathrm{B}}}\underline{\underline{\mathrm{X}}})\\ j\underline{\underline{\mathrm{B}}} & \underline{\underline{\mathrm{U}}}-\underline{\underline{\mathrm{B}}}\underline{\underline{\mathrm{X}}}\end{bmatrix}\begin{bmatrix}\underline{\mathrm{V}}\\ \underline{\mathrm{I}}\end{bmatrix}_{z=0^+}. \tag{25}$$

In the limit of the infinitely thin posts $\underline{\underline{\mathrm{X}}}\to 0$, and consequently, Eq. (25) is reduced to

$$\begin{bmatrix}\underline{\mathrm{V}}\\ \underline{\mathrm{I}}\end{bmatrix}_{z=0^-}=\begin{bmatrix}\underline{\underline{\mathrm{U}}} & 0\\ j\underline{\underline{\mathrm{B}}} & \underline{\underline{\mathrm{U}}}\end{bmatrix}\begin{bmatrix}\underline{\mathrm{V}}\\ \underline{\mathrm{I}}\end{bmatrix}_{z=0^+}, \tag{26}$$

in agreement with Ref. [38].

The matrices X and B, representing the reactive properties of a single unit cell, are used now in the dispersion analysis of the entire periodic waveguide with the Floquet theorem. In the general case of a nonzero X matrix, the dispersion equation of the periodic waveguide results in

$$\left\{\begin{bmatrix}\cos\left(\frac{1}{2}\underline{\underline{k}}_m\lambda_p\right) & j\sin\left(\frac{1}{2}\underline{\underline{k}}_m\lambda_p\right)\\ j\sin\left(\frac{1}{2}\underline{\underline{k}}_m\lambda_p\right) & \cos\left(\frac{1}{2}\underline{\underline{k}}_m\lambda_p\right)\end{bmatrix}\begin{bmatrix}\underline{\underline{\mathrm{U}}}-\underline{\underline{\mathrm{X}}}\underline{\underline{\mathrm{B}}} & j\underline{\underline{\mathrm{X}}}(2\underline{\underline{\mathrm{U}}}-\underline{\underline{\mathrm{B}}}\underline{\underline{\mathrm{X}}})\\ j\underline{\underline{\mathrm{B}}} & \underline{\underline{\mathrm{U}}}-\underline{\underline{\mathrm{B}}}\underline{\underline{\mathrm{X}}}\end{bmatrix}\begin{bmatrix}\cos\left(\frac{1}{2}\underline{\underline{k}}_m\lambda_p\right) & j\sin\left(\frac{1}{2}\underline{\underline{k}}_m\lambda_p\right)\\ j\sin\left(\frac{1}{2}\underline{\underline{k}}_m\lambda_p\right) & \cos\left(\frac{1}{2}\underline{\underline{k}}_m\lambda_p\right)\end{bmatrix}-e^{j\beta_0\lambda_p}\underline{\underline{\mathrm{U}}}\right\}\begin{bmatrix}\underline{\mathrm{V}}\\ \underline{\mathrm{I}}\end{bmatrix}=0, \tag{27}$$

where k_m is the diagonal matrix of the TE_{m0} mode wave numbers $\underline{\underline{k}}_m$.

Equation (27) is a matrix eigenvalue system. The eigenvectors

$$\begin{bmatrix}\underline{\mathrm{V}}\\ \underline{\mathrm{I}}\end{bmatrix},$$

which are the solutions of Eq. (27), describe the periodic transverse profiles of the periodic-waveguide modes. These modes are composed of linear superposition of TE_{m0} modes of the empty waveguide, which their relative amplitudes a_{mn} are specified by the dispersion equation (27), as

$$E_{xn}=\sum_{m=1}^{\infty}(a_{mn}^{+}\psi_m e^{-jk_{m}z}+a_{mn}^{-}\psi_m e^{jk_{m}z}), \tag{28}$$

where $\psi_m(y)=\sin[(\pi m/a)y]$ is the transverse profile of TE_{m0} mode. The corresponding eigenvalues β_{n0} of Eq. (27) are the fundamental wave numbers of the periodic-waveguide modes. The real and imaginary wave numbers correspond to the propagating and evanescent modes, respectively [38]. The Floquet theorem allows one to relate the forward and backward amplitudes $a_{mn}^{\pm}$ by

$$\frac{a_{mn}^{-}}{a_{mn}^{+}}=\frac{e^{-jk_m\lambda_p}-e^{-j\beta_{n0}\lambda_p}}{e^{-j\beta_{n0}\lambda_p}-e^{jk_m\lambda_p}}, \tag{29}$$

and Eq. (28) is rewritten in the form

$$E_{xn}=\sum_{m=1}^{\infty}a_{mn}^{+}\psi_m\left(e^{-jk_{m}z}+e^{jk_{m}z}\frac{e^{-jk_m\lambda_p}-e^{-j\beta_{n0}\lambda_p}}{e^{-j\beta_{n0}\lambda_p}-e^{jk_m\lambda_p}}\right). \tag{30a}$$

The magnetic field component of periodic-waveguide mode is obtained by Maxwell's equations as follows:

$$H_{yn}=\frac{1}{\omega\mu_0}\sum_{m=1}^{\infty}a_{mn}^{+}\psi_m k_m\left(e^{-jk_{m}z}-e^{jk_{m}z}\times\frac{e^{-jk_m\lambda_p}-e^{-j\beta_{n0}\lambda_p}}{e^{-j\beta_{n0}\lambda_p}-e^{jk_m\lambda_p}}\right). \tag{30b}$$

Each mode of the periodic waveguide forms its own infinite set of spatial harmonics,

$$E_{xn}=\sum_{k=-\infty}^{\infty} e_{nk}\psi_{nk}e^{-j\beta_{nk}z}, \tag{31a}$$

$$H_{yn}=\sum_{k=-\infty}^{\infty} h_{nk}\psi_{nk}e^{-j\beta_{nk}z}, \tag{31b}$$

where the kth harmonic wave number β_{nk} is defined by

$$\beta_{nk}=\beta_{n0}+\frac{2\pi k}{\lambda_p}. \tag{32}$$

The electric and magnetic harmonic coefficients are obtained from

$$e_{nk}\psi_{nk}=\frac{1}{\lambda_p}\int_0^{\lambda_p} E_{xn}e^{j\beta_{nk}z}dz, \tag{33a}$$

$$h_{nk}\psi_{nk}=\frac{1}{\lambda_p}\int_0^{\lambda_p} H_{yn}e^{j\beta_{nk}z}dz. \tag{33b}$$

Substitution of expressions (30) into Eqs. (33) results in the following relations for electric and magnetic harmonic coefficients:

$$e_{nk}\psi_{nk}=\frac{4j}{\lambda_p}\sum_{m=1}^{\infty} a_{mn}^{+}\psi_m\frac{k_m}{k_m^2-\beta_{nk}^2}\frac{\cos(k_m\lambda_p)-\cos(\beta_{n0}\lambda_p)}{e^{-j\beta_{n0}\lambda_p}-e^{jk_m\lambda_p}}, \tag{34a}$$

$$h_{nk}\psi_{nk}=\frac{4j\beta_{nk}}{\omega\mu_0\lambda_p}\sum_{m=1}^{\infty} a_{mn}^{+}\psi_m\frac{k_m}{k_m^2-\beta_{nk}^2}\times\frac{\cos(k_m\lambda_p)-\cos(\beta_{n0}\lambda_p)}{e^{-j\beta_{n0}\lambda_p}-e^{jk_m\lambda_p}}. \tag{34b}$$

The kth harmonic impedance is thus given by

$$Z_{nk}=\frac{e_{nk}\psi_{nk}}{h_{nk}\psi_{nk}}=Z_0\frac{k_0}{\beta_{nk}}. \tag{35}$$

The harmonic impedance (35) resembles the general expression for the TE mode impedance in a hollow waveguide, $Z=Z_0k_0/k_z$. This result stems from the fact that the periodic-waveguide mode is composed of only TE modes of the rectangular waveguide.

The harmonic impedance Z_{nk} is real for real β_{nk} in the nth-mode frequency passband, and is imaginary for imaginary β_{nk} in the stopband frequency region. The power flow of the kth spatial harmonic is derived using the orthogonality of TE modes, and results in

TABLE I. Parameters of the PWC-array model.

Waveguide parameters			
Total width	a	47	(mm)
Height	b	22	(mm)
Total length	L	0.5	(m)
Post diameter	d	1.5	(mm)
Axial period	λ_p	20	(mm)
Transverse period	p	9.5	(mm)
Electron beams			
Number of beams		1, 2, 3	
e-gun voltage	U_e	4	(kV)
Total current	I_e	0.2	(A)
Pitch ratio	$\overline{\beta_{e\perp}}/\overline{\beta_{ez}}$	2	
Axial magnetic field			
Fundamental mode	(A)	2.7	(kG)
Second mode	(B)	3.3	(kG)
Third mode	(C)	4.2	(kG)

$$p_{nk}=\frac{8ab}{\lambda_p^2 Z_{nk}}\sum_{m=1}^{\infty}|a_{mn}^{+}|^2\left|\frac{k_m}{k_m^2-\beta_{nk}^2}\right|^2\times\left|\frac{\cos(k_m\lambda_p)-\cos(\beta_{n0}\lambda_p)}{e^{-j\beta_{n0}\lambda_p}-e^{jk_m\lambda_p}}\right|^2. \tag{36}$$

The parameters resulting from the periodic-waveguide analysis above are used in the next section for numerical analysis of the CRM array.

IV. CRM-ARRAY AMPLIFICATION IN VARIOUS MODES

The CRM interaction with an array of electron beams in a 2D periodic waveguide is demonstrated in this section by several numerical examples. The CRM parameters used in these calculations are listed in Table I. The same parameters are used in the CRM-array experiment of Lei and Jerby [29].

The numerical results of the periodic-waveguide analysis are shown in Figs. 4 and 5. In these calculations, each mode of the periodic waveguide is expanded to the first 22 TE_{m0} modes of the rectangular waveguide (without the posts) to provide a satisfactory precision. The Brillouin diagram of the periodic waveguide is shown in Fig. 4. The calculations are conducted in the frequency range 6.5–12.5 GHz, which covers the first three modes of the periodic waveguide. The cutoff frequency of the first mode is found to be 6.9 GHz. The results show that only one mode may propagate in the waveguide for any given frequency in this range. Hence the periodic waveguide acts as a *mode selector* and it provides a single-mode operation even for the second- and third-order modes. Three-dimensional profiles of periodic-waveguide modes are plotted for the one unit cell in Figs. 5(a), 5(b), and 5(c) for the first, second, and third modes, respectively. The figures show that in the middle of the unit cell, the periodic-waveguide modes resemble the corresponding TE_{m0} modes of the empty waveguide, respectively. The higher modes of

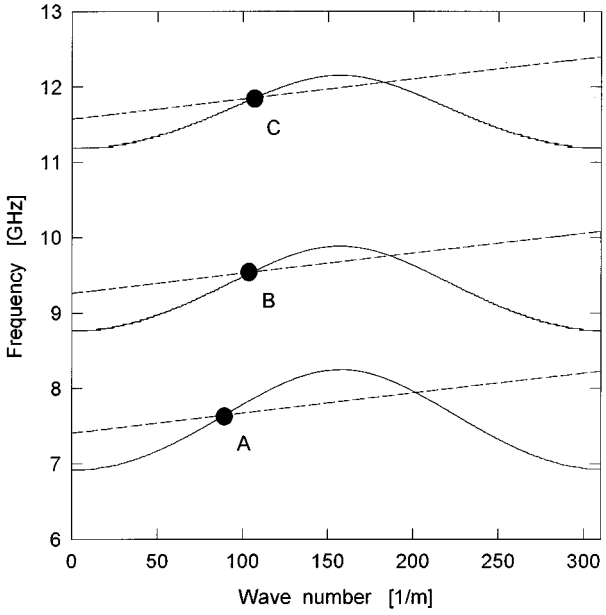

FIG. 4. The Brillouin diagram for the first three waveguide modes. The corresponding electron-beam lines [Eq. (1)] are shown in dashed lines.

rectangular waveguide become dominant in the vicinity of the metal posts.

The CRM interaction with the fundamental harmonics of the first three periodic-waveguide modes is computed numerically using Eqs. (18) and (19) (the weak coupling among the periodic-waveguide modes in the frequency range 6.9–12.5 GHz, enables a single-mode CRM interaction in this range). Figure 4 shows the interaction points of each one of these modes (points *A*, *B*, and *C* for the first, second, and third mode, respectively) with a 4 keV electron beam in different magnetic fields, as listed in Table I. For each periodic-waveguide mode, the interaction with one, two, and three electron beams is calculated. For the sake of comparison, the total electron current is taken the same for any number of beams in the array. The first 15 spatial harmonics are taken into account in the calculation of the power-flow ratio (15) of each mode. The computed power gains are presented in Figs. 6, 7, and 8 for interactions with one, two, and three electron beams, respectively. The maximum gains are plotted in Fig. 9 for each number of electron beams and periodic-waveguide mode orders. The results show that the largest gain is obtained by an interaction of one electron beam with the third mode of the periodic waveguide. This operating point is marked as *C* in the dispersion diagram in Fig. 4. Considerable gains are obtained also by a two electron-beam interaction with the second mode, and by a three electron-beam interaction with the third mode.

V. DISCUSSION

In this section we discuss the analysis of the multibeam CRM array presented above, and its implication for the development of new schemes of 2D and 3D CRM arrays.

Some of the principles of the CRM-array interaction are illustrated by Eq. (18) in the single-mode limit. The gain obtained by the CRM interaction depends on two factors: the

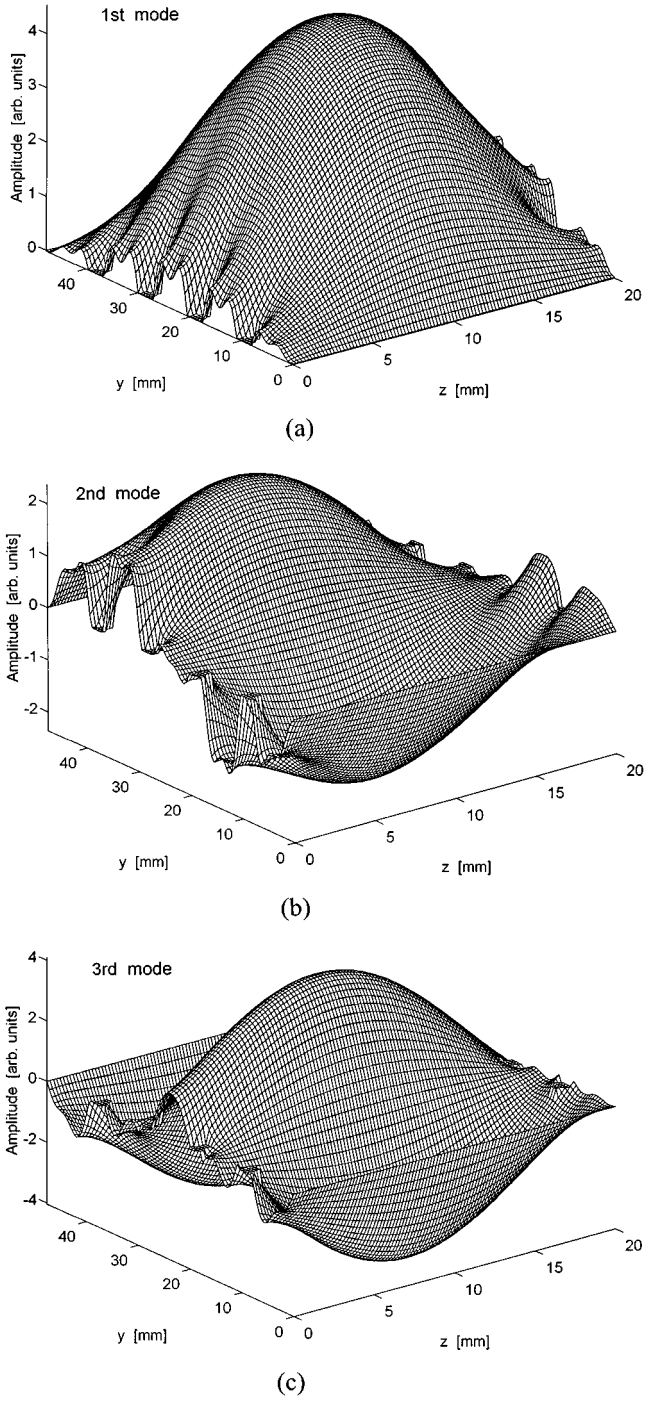

FIG. 5. Profiles of the first (a), second (b), and third (c) modes of the periodic waveguide in a unit cell.

coupling coefficient κ, and the filling factors $F_{f_{n0i}}$. The filling factors for given waveguide geometry depend on the position of electron beams inside the waveguide with respect to the spatial distribution of the radiation power. The coupling parameter (19) represents four mechanisms invloved in the CRM interaction as discussed in Refs. [5,24]. In the case where the initial electron velocity in the azimuthal direction is much smaller than the axial velocity, the CRM interaction has a nonbunching character [22]. In this case, the coupling parameter depends on the term $\hat{Z}_0 - \overline{\beta_{ez}}$. According to Eq.

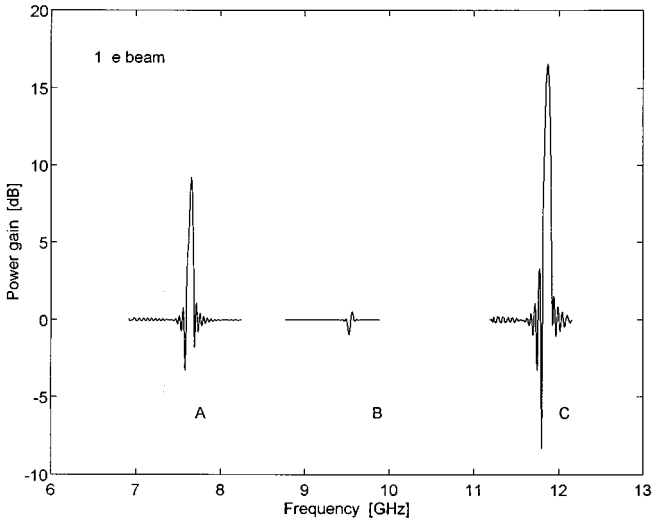

FIG. 6. Gain curves of a single electron-beam CRM interaction with the first (A), second (B), and third (C) modes. The corresponding axial magnetic fields are 2.7, 3.3, and 4.2 kG, respectively. The electron energy is 4 keV, the total electron current is 0.2 A, and the electron pitch ratio is $\beta_{e\perp}/\beta_{ez}=2$.

(35), this term is always positive for an interaction with fast TE waves ($\beta_{n0}<k_0$), and consequently, the CRM interaction in this case results in a radiation absorption [22,24]. The multibeam CRM interaction in a 2D periodic waveguide may provide slow-wave conditions ($\beta_{nk}>k_0$, $k\geqslant 1$) in high-order spatial harmonics. The anomalous Doppler effect in this case [20–22] may result in a positive gain without an initial rotation of the electron beams. This effect is a subject for further research.

The CRM bunching mechanisms become dominant when the electron beams are initially rotated at the entrance to the interaction region. The term $\hat{k}_0\hat{Z}_{n0}$ in expression (19) corresponds to the azimuthal bunching, whereas the term $\hat{\beta}_{n0}$ represents the axial bunching mechanism. These terms oppose one another, i.e., the azimuthal and the axial bunching effects tend to cancel one another. The azimuthal bunching dominates over the axial bunching effect in the fast-wave interaction, as with the fundamental harmonics presented above (where $\beta_{n0}<k_0$). Substituting Eq. (35) to the bunching coupling terms results in $(\hat{k}_0^2-\hat{\beta}_{n0}^2)/\hat{\beta}_{n0}$. Consequently, for a given fundamental wave number $\hat{\beta}_{n0}$, the azimuthal electron bunching becomes stronger as the frequency increases (whereas the axial bunching remains constant). The 2D periodic waveguide has an advantage in this respect that a single-mode operation is possible also with high modes (the fundamental passband of the third mode in the previous example exists in the stopbands of all other modes). This feature of the CRM array in a 2D periodic waveguide enables a

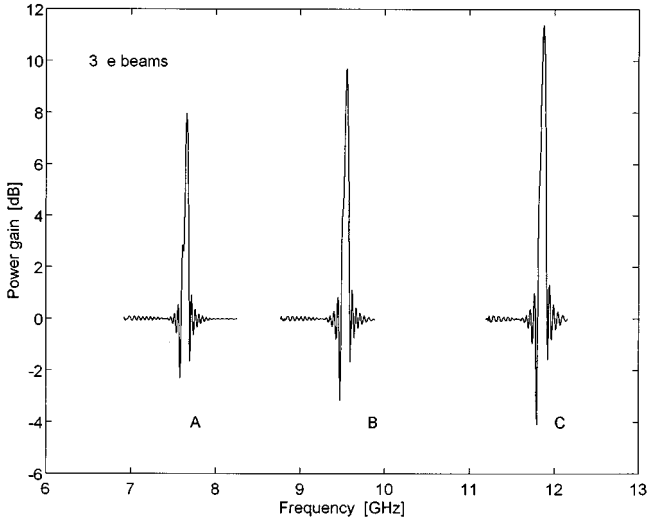

FIG. 8. Gain curves of a three electron-beam CRM interaction with the first (A), second (B), and third (C) modes. The magnetic fields and parameters of electron beams are the same as for Fig. 6.

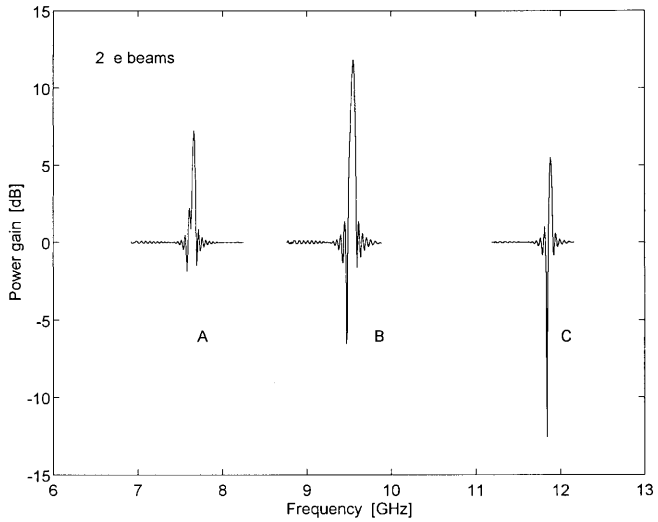

FIG. 7. Gain curves of a two electron-beam CRM interactions with the first (A), second (B), and third (C) modes. The magnetic fields and parameters of electron beams are the same as for Fig. 6.

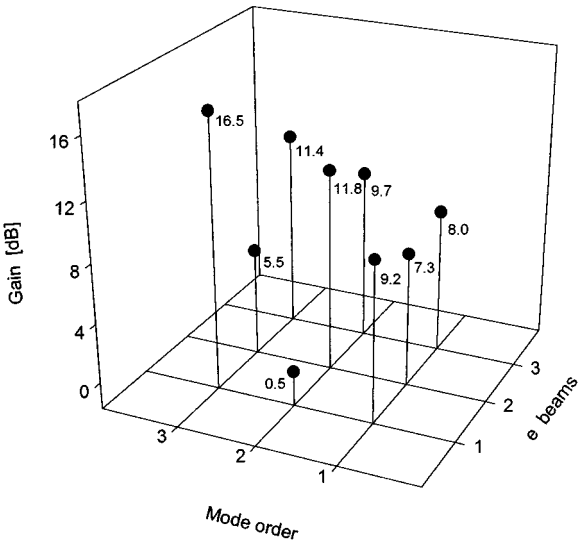

FIG. 9. Maximal gains of CRM-array interactions with various modes and different number of electron beams.

single-mode and near-cutoff operation, and consequently a stronger CRM interaction, in higher frequencies. The mode stability in the periodic waveguide and the wide cross section of the CRM-array interaction are consequent advantages.

Technical advantages of the CRM-array concept, resulting from the low-voltage operation, are related to the short collector section required for the low-energy electron beam, as compared to gyrotrons. The array structure also alleviates the difficulties associated with the radiation output window, which is a severe technical problem in gyrotron design. The emitted powers from different CRM-array channels can be summed up coherently in space as in phased-array antennas [37].

The multimode analysis of the multibeam CRM array in a 2D periodic waveguide will be used as a basis for the analysis of the experiment conducted by Lei and Jerby [29]. Further development of the theory of CRM arrays is planned in various directions, including multifrequency CRM emission, multiple CRM interactions and synergistic effects, 3D CRM arrays, and photonic-band-gap effects. We plan to discuss microwave radiators based on 3D CRM arrays with inherent features of phased-array antennas in a future paper [37].

The concept of the multibeam CRM array in multidimensional periodic structures [28] provides a basis for the development of low-voltage, high-power sources of microwave radiation.

ACKNOWLEDGMENTS

The authors thank Dr. V. Dichtiar for discussions on the periodic-waveguide analysis, and acknowledge support for this research by the Israel Science Foundation under Grant No. 724/94.

APPENDIX A: THE ELECTRON-BEAM FILLING FACTOR

The analytical expression for the product $F_{f_{nki}}p_{nk}$ defined by Eqs. (10) is derived in this appendix. This term describes the coupling between the ith electron beam and the kth spatial harmonic of the nth periodic-waveguide mode. The beam is assumed to be cylindrical and transversely uniform. Its transverse-profile function is defined by Eq. (7).

Substituting Eqs. (34a) and (34b) into Eq. (10b) results in

$$F_{f_{nki}}p_{nk}=\frac{16}{\lambda_p^2 Z_{nk}}\sum_{m=1}^{\infty}|a_{mn}^{+}|^2\left|\frac{k_m}{k_m^2-\beta_{nk}^2}\right|^2\left|\frac{\cos(k_m\lambda_p)-\cos(\beta_{n0}\lambda_p)}{\exp(-j\beta_{n0}\lambda_p)-\exp(jk_m\lambda_p)}\right|^2\int_{S_i}\sin^2\left(\frac{\pi m}{a}y\right)dxdy, \tag{A1}$$

where S_i is the ith electron beam cross section. The integral in the right side of Eq. (A1) is rewritten in the form

$$\int_{S_i}\sin^2\left(\frac{\pi m}{a}y\right)dxdy=\frac{1}{2}\pi r_{0i}^2-\frac{1}{2}\cos\left(\frac{2\pi m}{a}y_{0i}\right)\int_0^{2\pi}d\varphi\int_0^{r_{0i}}rdr\cos\left(\frac{2\pi mr}{a}\sin\varphi\right)$$
$$+\frac{1}{2}\sin\left(\frac{2\pi m}{a}y_{0i}\right)\int_0^{2\pi}d\varphi\int_0^{r_{0i}}rdr\sin\left(\frac{2\pi mr}{a}\sin\varphi\right), \tag{A2}$$

where r and φ are the polar coordinates associated with the ith electron beam cross section. The last term in Eq. (A2) vanishes, since its integrand is an odd function of φ with a period of 2π. After some algebraic steps, Eq. (A2) results in

$$\int_{S_i}\sin^2\left(\frac{\pi m}{a}y\right)dxdy=r_{0i}^2\left(\frac{\pi}{2}-2\cos\left(\frac{2\pi m}{a}y_{0i}\right)\int_0^{\pi/2}d\varphi\left\{\frac{a}{2\pi mr_{0i}\sin\varphi}\sin\left(\frac{2\pi mr_{0i}}{a}\sin\varphi\right)\right.\right.$$
$$\left.\left.+\left(\frac{a}{2\pi mr_{0i}\sin\varphi}\right)^2\left[\cos\left(\frac{2\pi mr_{0i}}{a}\sin\varphi\right)-1\right]\right\}\right). \tag{A3}$$

An expansion of the sine and cosine functions to the Taylor series gives

$$\int_{S_i}\sin^2\left(\frac{\pi m}{a}y\right)dxdy=r_{0i}^2\left\{\frac{\pi}{2}-\cos\left(\frac{2\pi m}{a}y_{0i}\right)\sum_{l=0}^{\infty}\frac{(-1)^l}{(2l)!(l+1)}\left(\frac{2\pi mr_{0i}}{a}\right)^{2l}\int_0^{\pi/2}(\sin\varphi)^{2l}d\varphi\right\}. \tag{A4}$$

The solution of the integral in the left side of Eq. (A4) is known as

$$\int_0^{\pi/2}(\sin\varphi)^{2l}d\varphi=\frac{\pi}{2}\frac{(2l-1)!!}{(2l)!!}, \tag{A5}$$

where the the double factorial is defined by

$$N!!=\begin{cases}1\times3\times5\times\cdots\times N, & N=1,3,5,\ldots\\ 2\times4\times6\times\cdots\times N, & N=2,4,6,\ldots.\end{cases} \tag{A6}$$

Finally, Eq. (A2) results in

$$\int_{S_i} \sin^2\left(\frac{\pi m}{a} y\right) dx dy = \frac{1}{2}\pi r_{0i}^2 \left\{ 1 - \cos\left(\frac{2\pi m}{a} y_{0i}\right) \sum_{l=0}^{\infty} \left(\frac{\pi m r_{0i}}{a}\right)^{2l} \frac{(-1)^l}{l!(l+1)!} \right\}, \tag{A7}$$

which gives the following expression for the product $F_{f_{nki}} p_{nk}$,

$$F_{f_{nki}} p_{nk} = \frac{8\pi r_{0i}^2}{\lambda_p^2 Z_{nk}} \sum_{m=1}^{\infty} |a_{mn}^{+}|^2 \left| \frac{k_m}{k_m^2 - \beta_{nk}^2} \right|^2 \left| \frac{\cos(k_m \lambda_p) - \cos(\beta_{n0}\lambda_z)}{\exp(-j\beta_{n0}\lambda_p) - \exp(jk_m\lambda_p)} \right|^2 \left\{ 1 - \cos\left(\frac{2\pi m}{a} y_{0i}\right) \sum_{l=0}^{\infty} \left(\frac{\pi m r_{0i}}{a}\right)^{2l} \frac{(-1)^l}{l!(l+1)!} \right\}. \tag{A8}$$

This expression is used in this work as the electron-beam filling factor in the analysis of the multibeam CRM array.

APPENDIX B: THE REFLECTION-COEFFICIENT MATRIX OF A SINGLE ROW OF POSTS

The analysis of the periodic waveguide is based on the features of its unit cell. In this appendix, the reflection coefficient matrix of a single row of posts is derived.

Figure 2 shows the horizontal cross section of the waveguide. The unit cell is considered as a transverse row of posts placed at $z=0$, as shown in Fig. 3(a). All posts have the equal diameter d and they are assumed to be perfectly conducting. The posts are numbered from $-K$ to K. The zero number corresponds to the central post that may or may not be present. The y coordinate of the νth post center and the polar angle are ρ_ν and ϕ, respectively, as shown in Fig. 2. The surface of the νth post is expressed in polar coordinates ρ_ν and ϕ by

$$y_0 = \rho_\nu - \frac{1}{2} d\cos\phi, \tag{B1a}$$

$$z_0 = \frac{1}{2} d\sin\phi. \tag{B1b}$$

The electric field incident to the posts is defined by Eqs. (20)–(22). On the surface of the νth post this field is given by

$$E_{x\nu}^{(i,o/e)} = \sum_{m=1}^{\infty} a_m^{(o/e)} \sum_{k=-\infty}^{\infty} J_k\left(\frac{1}{2}k_0 d\right) e^{jk\phi} \left[\sin\left(\frac{\pi m}{a}\rho_\nu - k\phi_m\right) \mp (-1)^k \sin\left(\frac{\pi m}{a}\rho_\nu + k\phi_m\right) \right], \tag{B2}$$

which is a superposition of angular harmonics numerated by the integer k, where $J_k(Z)$ is the Bessel function of the first kind of order k, and the parameter ϕ_m is defined for each mth mode by

$$e^{j\phi_m} = \frac{1}{k_0}\left(k_m + j\frac{\pi m}{a}\right). \tag{B3}$$

The parameter ϕ_m is real for the propagating mode and complex for the evanescent one.

The surface currents induced on the posts have no variation in x. Then, making use of the common imaging technique, we assume that (1) the posts are infinitely long in the x direction, (2) the post array is infinite in the y direction, and consequently, (3) the post locations and current distributions in each transverse unit cell of width a are the consecutive mirror images of each other. These assumptions replace the waveguide walls, since the same boundary conditions are automatically fulfilled.

The scattered field generated in the point (y,z) by the linear current $I_x(y_0,z_0)$ is given by

$$E_x^{(s)}(y,z) = -\frac{j\omega\mu_0}{4\pi} I_x(y_0,z_0) \int_{-\infty}^{\infty} \frac{e^{-jk_0[x_0^2+(y-y_0)^2+(z-z_0)^2]^{1/2}}}{[x_0^2+(y-y_0)^2+(z-z_0)^2]^{1/2}} dx_0 = -\frac{\omega\mu_0}{4} I_x(y_0,z_0) H_0^{(2)}[k_0[(y-y_0)^2+(z-z_0)^2]^{1/2}], \tag{B4}$$

where $H_0^{(2)}$ is the Hankel function of the second kind of order 0. The total scattered field is obtained by integrating over the post surface and summing over all posts. Making use of the polar coordinates introduced in Fig. 2 results in

$$E_x^{(s)}(y,z) = -\frac{\omega\mu_0}{4} \sum_{m=1}^{\infty} \sum_{\mu=-K}^{K} \int_0^{2\pi} I_{m\mu}(\psi) \sum_{l=-\infty}^{\infty} (-1)^{ml} H_0^{(2)}\left\{ k_0 \left[\left(y + la - \rho_\mu + \frac{1}{2}d\cos\psi\right)^2 + \left(z - \frac{1}{2}d\sin\psi\right)^2 \right]^{1/2} \right\} d\psi, \tag{B5}$$

where $I_{m\mu}$ is the current element generated on the μth post by the mth incident mode and ψ is the polar angle of the point y_0, z_0 on the surface of this post. The scattered field on the surface of the νth post is

$$E_{x\nu}^{(s)}(\phi)=-\frac{\pi\omega\mu_0}{2}\sum_{m=1}^{\infty}\sum_{k=-\infty}^{\infty}J_k\left(\frac{1}{2}k_0d\right)e^{jk\phi}\left\{\sum_{\mu=-K}^{K}\sum_{i=-\infty}^{\infty}\left[J_n\left(\frac{1}{2}k_0d\right)I_{m\mu n}f_{m,n-k}(\rho_\mu-\rho_\nu)\right]+H_k^{(2)}\left(\frac{1}{2}k_0d\right)I_{m\nu k}\right\}, \tag{B6}$$

where

$$I_{m\mu n}=\frac{1}{2\pi}\int_0^{2\pi}I_{m\mu}(\psi)e^{-jn\psi}d\psi, \tag{B7a}$$

are the angular harmonic coefficients of the discrete Fourier series

$$I_{m\mu}(\psi)=\sum_{n=-\infty}^{\infty}I_{m\mu n}e^{jn\psi}, \tag{B7b}$$

and the function f is defined by

$$f_{m,\alpha}(Z)=\sum_{\substack{l=-\infty\\ Z+la\neq 0}}^{\infty}(-1)^{ml}H_\alpha^{(2)}(k_0|Z+la|)\mathrm{sgn}^\alpha(Z+la). \tag{B8}$$

The total electric field is a sum of incident and scattered fields, and it must vanish on the post surface. Hence for the surface of the νth post we have

$$\sum_{m=1}^{\infty}a_m^{(o/e)}\sum_{k=-\infty}^{\infty}J_k\left(\frac{1}{2}k_0d\right)e^{jk\phi}\left[\sin\left(\frac{\pi m}{a}\rho_\nu-k\phi_m\right)\mp(-1)^k\sin\left(\frac{\pi m}{a}\rho_\nu+k\phi_m\right)\right]$$
$$=\frac{\pi\omega\mu_0}{2}\sum_{m=1}^{\infty}\sum_{k=-\infty}^{\infty}J_k\left(\frac{1}{2}k_0d\right)e^{jk\phi}\left\{\sum_{\mu=-K}^{K}\sum_{n=-\infty}^{\infty}\left[J_n\left(\frac{1}{2}k_0d\right)I_{m\mu n}^{(o/e)}f_{m,n-k}(\rho_\mu-\rho_\nu)\right]+H_k^{(2)}\left(\frac{1}{2}k_0d\right)I_{m\nu k}^{(o/e)}\right\}. \tag{B9}$$

Equation (B9) can be further simplified by use of general properties: the linear independence of modes, and the uniqueness of the Fourier series. Consequently, $\Sigma_m\Sigma_k J_k(\frac{1}{2}k_0d)e^{jk\phi}$ may be removed from both sides of Eq. (B9), which results in

$$\sum_{\mu=-K}^{K}\sum_{n=-\infty}^{\infty}\left[J_n\left(\frac{1}{2}k_0d\right)\left\{\frac{I_{m\mu n}^{(o/e)}}{a_m^{(o/e)}}\right\}f_{m,n-k}(\rho_\mu-\rho_\nu)\right]+H_k^{(2)}\left(\frac{1}{2}k_0d\right)\left\{\frac{I_{m\nu k}^{(o/e)}}{a_m^{(o/e)}}\right\}$$
$$=\frac{2}{\pi\omega\mu_0}\left[\sin\left(\frac{\pi m}{a}\rho_\nu-k\phi_m\right)\mp(-1)^k\sin\left(\frac{\pi m}{a}\rho_\nu+k\phi_m\right)\right]. \tag{B10}$$

Equation (B10) is satisfied for each even or odd mode m, post number ν, and angular harmonic k. Consequently, for M interacting modes there are $2M$ systems of linear equations. The order of each system is the number of posts times the number of angular harmonics. All the coefficients $\{I_{m\mu k}^{(o/e)}/a_m^{(o/e)}\}$ can be calculated from these systems of equations. In addition, since the current generated by the mth mode at any point on the post surface is proportional to the incident field in this point, then the use of Eq. (21) results in the symmetry relations

$$\left\{\frac{I_{m\mu-k}^{(o/e)}}{a_m^{(o/e)}}\right\}=\mp\left\{\frac{I_{m\mu k}^{(o/e)}}{a_m^{(o/e)}}\right\}, \tag{B11a}$$

$$\left\{\frac{I_{m-\mu k}^{(o/e)}}{a_m^{(o/e)}}\right\}=\pm(-1)^{k+m}\left\{\frac{I_{m\mu k}^{(o/e)}}{a_m^{(o/e)}}\right\}. \tag{B11b}$$

In particular, for the zero harmonic and the central post $\nu=0$, these result in

$$\left\{\frac{I_{m\mu 0}^{(o)}}{a_m^{(o)}}\right\}=0, \tag{B11c}$$

$$\left\{ \frac{I_{m0k}^{(o/e)}}{a_m^{(o/e)}} \right\}_{k+m=\text{odd/even number}} = 0. \tag{B11d}$$

The current coefficients defined by Eqs. (B10) and (B11) are used further in this section in order to determine the reflection coefficients of the unit cell of periodic waveguide. At a large distance from the posts, namely, if $|z| > \frac{1}{2}d$, the scattered field given by Eq. (B5) may be expanded to an infinite series of empty waveguide modes as follows:

$$E_x^{(s)}(y,z) = -\frac{2\pi\omega\mu_0}{a} \sum_{\mu=-K}^{K} \sum_{n=-\infty}^{\infty} (-1)^n J_n\left(\frac{1}{2}k_0 d\right) \left[\sum_{m,m'=1,3,\ldots}^{\infty} I_{m\mu n} \frac{1}{k_{m'}} e^{-jk_{m'}z} \cos\left(\frac{\pi m'}{a}(y-\rho_\mu) - n\phi_{m'}\right) \right.$$
$$\left. + \sum_{m,m'=2,4,\ldots}^{\infty} I_{m\mu n} \frac{1}{k_{m'}} e^{-jk_{m'}z} \cos\left(\frac{\pi m'}{a}(y-\rho_\mu) - n\phi_{m'}\right) \right]. \tag{B12}$$

The scattered field is divided into the symmetric and antisymmetric parts (odd and even numbers m, m', respectively). It is a consequence of the waveguide transverse symmetry. The total electric field is a sum of incident and scattered waves, and it is given by

$$E_x^{(o/e)}(y,z) = \sum_{m=1}^{\infty} a_m^{(o/e)} \sin\left(\frac{\pi m}{a}y\right)(e^{jk_m z} \mp e^{-jk_m z}) - \frac{2\pi\omega\mu_0}{a} \sum_{\mu=-K}^{K} \sum_{n=-\infty}^{\infty} (-1)^n J_n\left(\frac{1}{2}k_0 d\right)$$
$$\times \left[\sum_{m,m'=1,3,\ldots}^{\infty} \sin\left(\frac{\pi m'}{a}y\right) I_{m\mu n}^{(o/e)} \frac{1}{k'} e^{-jk_{m'}z} \sin\left(\frac{\pi m'}{a}\rho_\mu + n\phi_{m'}\right) \right.$$
$$\left. + \sum_{m,m'=2,4,\ldots}^{\infty} \sin\left(\frac{\pi m'}{a}y\right) I_{m\mu n}^{(o/e)} \frac{1}{k'} e^{-jk_{m'}z} \sin\left(\frac{\pi m'}{a}\rho_\mu + n\phi_{m'}\right) \right]. \tag{B13}$$

The symmetry properties (B11) are used in the derivation of Eq. (B13).

The matrix of reflection coefficients R is introduced in Ref. [38] for the multimode interaction. The element $R_{m',m}$ of this matrix is defined as a reflection coefficient of m'th mode due to the mth incident mode. Thus the reflection coefficients for odd and even mode at $z=0$ are defined from Eq. (B13) by

$$R_{m'm}^{(o/e)} \sin\left(\frac{\pi m}{a}y\right) = \mp \sin\left(\frac{\pi m}{a}y\right)\delta_{m'm} - \frac{2\pi\omega\mu_0}{ak_{m'}} \sin\left(\frac{\pi m'}{a}y\right) \sum_{\mu=-K}^{K} \sum_{n=-\infty}^{\infty} (-1)^n J_n\left(\frac{1}{2}k_0 d\right) \left\{ \frac{I_{m\mu n}^{(o/e)}}{a_m^{(o/e)}} \right\} \sin\left(\frac{\pi m'}{a}\rho_\mu + n\phi_{m'}\right), \tag{B14}$$

and the matrix elements $R_{m'm}$ for different m, m' are obtained as follows:

$$R_{m'm}^{(o/e)} = 0, \quad m + m' = 3,5,\ldots, \tag{B15a}$$

$$R_{mm}^{(o/e)} = \mp 1 - \frac{2\pi\omega\mu_0}{ak_m} \sum_{\mu=-K}^{K} \sum_{n=-\infty}^{\infty} (-1)^n J_n\left(\frac{1}{2}k_0 d\right)$$
$$\times \left\{ \frac{I_{m\mu n}^{(o/e)}}{a_m^{(o/e)}} \right\} \sin\left(\frac{\pi m}{a}\rho_\mu + n\phi_m\right), \tag{B15b}$$

and

$$R_{m'm}^{(o/e)} = |R_{m'm}^{(o/e)}| \exp(j\Phi_{m'm}^{(o/e)}), \quad m \neq m' \tag{B15c}$$

where the module $|R_{m'm}^{(o/e)}|$ and phase angle $\Phi_{m'm}^{(o/e)}$ are given by

$$|R_{m'm}^{(o/e)}| = \frac{2\pi\omega\mu_0}{a} |D_{m'm}| \tag{B16a}$$

and

$$\Phi_{m'm}^{(o/e)} = \tan^{-1}\left(\frac{\mathrm{Im}(D_{m'm})}{\mathrm{Re}(D_{m'm})}\right), \tag{B16b}$$

respectively, and the parameter $D_{m'm}$ is defined by

$$D_{m'm} = \frac{1}{k_{m'}} \sum_{\mu=-K}^{K} \sum_{n=-\infty}^{\infty} (-1)^n J_n\left(\frac{1}{2}k_0 d\right)$$
$$\times \left\{ \frac{I_{m\mu n}^{(o/e)}}{a_m^{(o/e)}} \right\} \sin\left(\frac{\pi m}{a}\rho_\mu + n\phi_m\right). \tag{B17}$$

These reflection-coefficient matrices are used in Eqs. (23a) and (23b) for calculating the equivalent transmission-line parameters.

[1] *High Power Microwave Sources*, edited by V. L. Granatstein and I. Alexeff (Artech House, Boston, 1987).
[2] J. Benford and J. Swegle, *High-Power Microwaves* (Artech House, Boston, 1992).
[3] J. L. Hirshfield and V. L. Granatstein, IEEE Trans. Microwave Theory Tech. **25**, 522 (1977), and references therein.
[4] V. A. Flyagin, A. V. Gaponov, M. I. Petelin, and V. K. Yulpatov, IEEE Trans. Microwave Theory Tech. **MTT-25**, 514 (1977).
[5] K. R. Chu and J. L. Hirshfield, Phys. Fluids **21**, 461 (1978), and references therein.
[6] A. W. Fliflet and W. M. Manheimer, Phys. Rev. A **39**, 3432 (1989).
[7] G. S. Nusinovich and Nai Li, IEEE Trans. Plasma Sci. **20**, 170 (1992).
[8] A. Bondeson, B. Levush, W. M. Manheimer, and E. Ott, Int. J. Electron. **53**, 547 (1982).
[9] D. S. Furuno, D. B. McDermott, H. Cao, C. S. Kou, N. C. Luhmann, Jr., P. Vitello, and K. Ko, Int. J. Electron. **65**, 429 (1988).
[10] G. P. Saraph, W. Lawson, M. Castle. J. Cheng, J. P. Calame, and G. S. Nusinovich, IEEE Trans. Plasma Sci. **24**, 671 (1996).
[11] H. Z. Guo, V. L. Granatstein, T. M. Antonsen, Jr., B. Levush, J. Tate, and S. H. Chen (unpublished).
[12] N. S. Ginzburg, I. V. Zotova, I. V. Konoplev, A. S. Sergeev, V. G. Shpak, S. A. Shunailov, M. R. Ul'maskulov, and M. I. Yalandin, Pis'ma Zh. Éksp. Teor. Fiz. **63**, 322 (1996) [JETP Lett. **63**, 331 (1996)].
[13] V. L. Granatstein, M. Herndon, R. K. Parker, and S. P. Shlesinger, IEEE Trans. Microwave Theory Tech. **MTT-22**, 1000 (1974).
[14] V. L. Granatstein, M. Herndon, P. Sprangle, Y. Carmel, and J. A. Nation, Plasma Phys. **17**, 23 (1975).
[15] S. G. Tantawi, W. T. Main, P. E. Latham, G. S. Nusinovich, W. G. Lawson, C. D. Striffler, and V. L. Granatstein, IEEE Trans. Plasma Sci. **20**, 205 (1992).
[16] J. M. Baird, S. Y. Park, K. R. Chu, H. Keren, and J. L. Hirshfield, Bull. Am. Phys. Soc. **25**, 911 (1980).
[17] K. R. Chu, A. K. Ganguly, V. L. Granatstein, J. L. Hirshfield, S. Y. Park, and J. M. Baird, Int. J. Electron. **51**, 493 (1981).
[18] M. Einat, E. Jerby, and A. Shahadi, Nucl. Instrum. Methods Phys. Res. A **375**, 22 (1996); M. Einat and E. Jerby (unpublished).
[19] E. S. Weibel, Phys. Rev. Lett. **2**, 83 (1959).
[20] S. Yu. Galuzo, V. I. Kanavets, A. I. Slepkov, and V. A. Pletyushkin, Zh. Tekh. Fiz. **52**, 1681 (1982) [Sov. Phys. Tech. Phys. **27**, 1030 (1982)].
[21] A. N. Didenko, A. R. Borisov, G. P. Fomenko, A. S. Shlapakovskii, and Yu. G. Shtein, Pis'ma Zh. Tekh. Fiz. **9**, 1331 (1983) [Sov. Tech. Phys. Lett. **9**, 572 (1983)].
[22] M. V. Kuzelev and A. A. Rukhadze, Usp. Fiz. Nauk **152**, 285 (1987) [Sov. Phys. Usp. **30**, 507 (1987)].
[23] E. Jerby and G. Bekefi, Phys. Rev. E **48**, 4637 (1993).
[24] E. Jerby, Phys. Rev. E **49**, 4487 (1994), and references therein.
[25] M. Korol and E. Jerby, Nucl. Instrum. Methods Phys Res. A **375**, 222 (1996).
[26] E. Jerby, G. Bekefi, and A. Shahadi, Nucl. Instrum. Methods Phys. Res. A **341**, 115 (1995).
[27] E. Jerby, A. Shahadi, V. Grinberg, V. Dichtiar, M. Sheinin, E. Agmon, H. Golombek, V. Trebich, M. Bensal, and G. Bekefi, IEEE J. Quantum Electron. **31**, 970 (1995).
[28] E. Jerby (unpublished).
[29] Li Lei and E. Jerby, Proc. SPIE **30**, 2843 (1996).
[30] M. E. Read, G. Nusinovich, O. Dumbrajs, G. Bird, J. P. Hogge, K. Kreischer, and M. Blank, IEEE Trans. Plasma Sci. **24**, 586 (1996).
[31] V. L. Bratman, G. G. Denisov, B. D. Kol'chugin, S. V. Samsonov, and A. B. Volkov, Nucl. Instrum. Methods Phys. Res. A **375**, 360 (1996).
[32] G. Bekefi, J. Appl. Phys. **71**, 4128 (1992).
[33] R. B. Palmer, R. C. Fernow, J. Fischer, J. C. Gallardo, H. G. Kirk, S. Ulc, H. Wang, Y. Zhao, K. Eppley, W. Herrmannsfeldt, R. Miller, and D. Yu, Nucl. Instrum. Methods Phys. Res. A **366**, 1 (1995).
[34] V. Dichtiar and E. Jerby (unpublished).
[35] E. Yablonovich, T. J. Gmitter, K. M. Leung, R. D. Meade, A. M. Rappe, K. D. Brommer, and J. D. Joannopoulos, Opt. Quantum Electron. **24**, S273 (1992).
[36] E. Jerby, Phys. Rev. A **41**, 3804 (1990).
[37] E. Jerby *et al.* (unpublished).
[38] R. E. Collin, *Field Theory of Guided Waves* (McGraw-Hill, New York, 1960).
[39] T. A. Abele, Bell Syst. Tech. J. **57**, 577 (1978), and references therein.